Spatially resolved ion density measurements in atmospheric oxyfuel flames using a spinning disc Langmuir probe

C. R. Martin
Assistant Professor of Mechanical Engineering
Penn State Altoona

June 15, 2019

1 Introduction

The works of Clements and Smy on Langmuir probes in dense plasmas [] establish that the probe's saturation current density is a function of its diameter, the fluid velocity, and the local ion density. For a given wire diameter and fluid velocity, we may infer the ion density from the measured current.

Unfortnately, for a wire injected into a plasma where ion density cannot be assumed constant along its length, it is not possible to distinguish between currents accumulated from base to tip. Calcote et al. used elaborate methods to insulate and cool wires up to the tip, where the measurement is taken [], but in the extreme thermal loads observed in atmospheric oxyfuel flames, even these efforts would be doomed. Good spatial resolution without severe disturbance to the flow demands that probes be tiny in diameter, but the surface-area to cross-sectional area ratio diverges in these geometries. While this observation makes it all the more impressive that efforts to construct a stationary probe for spatial measurements ever succeeded at all, it compells us to look for alternative methods in atmospheric flames.

If the probe is to be un-cooled, then its time in the flame must be very limited lest it be destroyed. The imagination may conjure rapid linear injection along the probe's length, but a wire mounted on a disc like was demonstrated by MacLatchey [] is far more mechanically elegant. Section 2 addresses the design of a disc to preserve such a probe.

Regardless of how it is injected into the flame, if the probe is a small uninsulated wire, then the measured currents will be an integral of all the currents along its length. How is it possible to make spatially resolved measurements? Inspiration may be drawn from tomography and Abel transformation (i.e. "onion peeling") methods, which elegantly address the problem of inferring some spatially distributed property from a plurality of integrated line-of-sight measurements. We develop a framework for deconvolving the measurements numerically in Section **??**.

2 Disc speeds

Over the course of its rotation, the wire will spend the vast majority of its time bathed in ambient air. It will only be subjected to the intense heat of the oxyfuel flame for a brief interval. This section is devoted to predicting how well such an arrangement will protect the wire from destruction due to melting.

A wire of diameter, D_w, length, L, with specific heat, c, and density, ρ, undergoing convection with a coefficient, h, will heat according to the equation

$$\rho c \frac{L\pi {D_w}^2}{4} \dot{T} = \pi D_w L h \left(T_{amb} - T \right).$$

or simply

$$\frac{\rho c D_w}{4h} \dot{T} + T = T_{amb}. \tag{1}$$

Nichrome steel enjoys a high mechanical strength, relatively high density (7,900 kg/m^3), relatively high specific heat (500J/kg-K) and favorable resistance to corrosion. If the convective coefficient were aggressively approximated on the order of 1000W/m^2-K for a 0.25mm (0.01in) diameter wire, then the time constant, τ, of Equation 1 is about one quarter (0.25) seconds.

After sufficient time has passed that the wire has taken many journeys through the flame, its temperature prior to entering will converge to some constant, and the temperature response will converge to a piecewise solution. If the wire is emersed in the flame for an interval, t_f, and requires t_c seconds to rotate, then

$$\tau \dot{T} + T = T_{flame} \qquad 0 \le t < t_f \tag{2a}$$

$$\tau \dot{T} + T = T_{amb} \qquad t_f \le t \le t_c \tag{2b}$$

with the boundary condition that $T(0) = T(t_c)$. It will become quite convenient to non-dimensionalize the temperatures by scaling

$$k = \frac{T - T_{amb}}{T_{flame} - T_{amb}}. \tag{3}$$

so equations 2 become

$$\tau\dot{k} + k = 1 \qquad 0 \le t < t_f \tag{4a}$$

$$\tau\dot{k} + k = 0 \qquad t_f \le t \le t_c \tag{4b}$$

The solutions are

$$k(t) = \begin{cases} (k_{min} - 1)\exp(-t/\tau) + 1 & 0 \le t < t_f \\ k_{max}\exp(-(t - t_f)/\tau) & t_f \le t \le t_c \end{cases} \tag{5}$$

when k_{min} and k_{max} are the temperatures prior to and after the wire's passage through the flame respectively. We solve for them by asserting that

$$k_{max} = (k_{min} - 1)\exp(-t_f/\tau) + 1$$
$$k_{min} = k_{max}\exp(-(t_c - t_f)/\tau)$$

when t_f is the time the wire dwells in the flame, t_c is the period of rotation. The time that the wire spends in the ambient, $t_a = t_c - t_f$, appears naturally. Solving for k_{min} and k_{max},

$$k_{max} = \frac{1 - \exp(-t_f/\tau)}{1 - \exp(-t_c/\tau)} \tag{6a}$$

$$k_{min} = \frac{\exp(-t_a/\tau) - \exp(-t_c/\tau)}{1 - \exp(-t_c/\tau)} \tag{6b}$$

The times, t_c, t_a, and t_f, are determined by the rotation frequency, f and the fraction, $\chi = t_f/t_c$, of the disc's motion that places the wire in the flame.

$$t_c = \frac{1}{f} \qquad t_f = \frac{\chi}{f} \qquad t_a = \frac{1 - \chi}{f}$$

We may expand the exponentials of equation 6a to obtain a simpler estimate for the maximum temperature,

$$k_{max} \approx \chi\frac{2f\tau - \chi}{2f\tau - 1}. \tag{7}$$

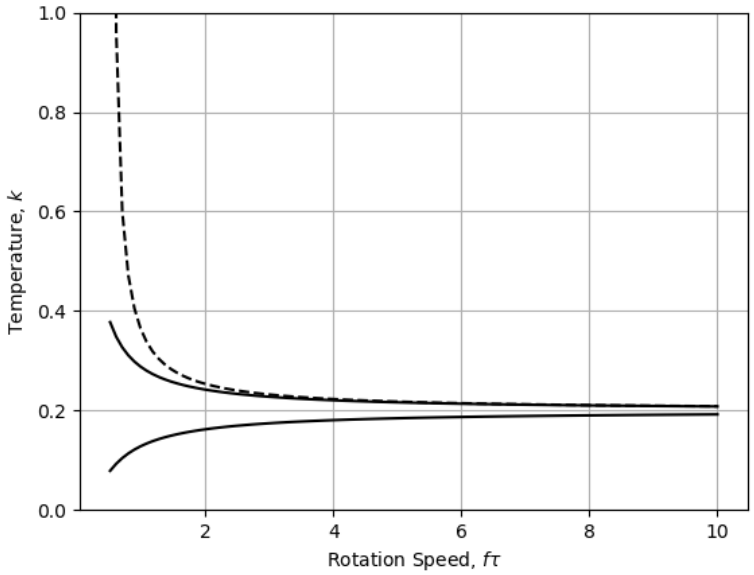

Figure 1: Maximum and minimum d-less temperatures versus d-less disc speed for $\chi = 0.2$. The dashed line is the approximate k_{max} from Equation 7

Clearly, in the limit where $f\tau \gg 1$, $k_{max} \to \chi$.

Figure 1 shows the dimensionless temperatures k_{max} and k_{min} versus disc speed, and the approximate k_{max} is plotted with a dashed line. The choice of $\chi = 0.2$ is consistent with a flame approximately 12mm (0.5in) across with a wire radius of 100mm (4in).

Since χ will be constant for a given flame and disc geometry, and k_{max} is a constraint based on the melting temperature of the wire, we may calculate a minimum safe disc speed. When we use the expansion in Equation 7, we will produce a conservative calculation for f that cannot be less than $1/2\tau$ due to the singularity in the expansion.

$$f > \left(\frac{1}{2\tau}\right)\left(\frac{k_{max} - \chi^2}{k_{max} - \chi}\right) \tag{8}$$

If the flame temperature were about 3000K, the wire melting temperature were about 1700K, and the ambient were about 300K, then $k_{max} = 0.52$, and the minimum disc speed is $f > 0.75/\tau$. If τ is 0.25s, then the disc should spin at least three rotations per second (180rpm).

While this is a modest speed for a spinning disc, it should be emphasized that the estimates for the peak wire temperature may be regarded as quite aggressive. Firstly, all additional cooling due to radiation or conduction along the wire length have been neglected. Moreover, the expansion used in forming Equation 7 is inherently pessimistic as shown in Figure 1. The only cause for concern that higher wire temperatures may be possible seems to be that the convection in the flame could be more severe than the convection in the ambient.

Regardless, a 200mm (8in) diameter disc spinning at about 70 revolutions per second (about 400rpm) should be far in excess of what is required to protect a 0.25mm (.01in) diameter wire. Such a system would propel the wire at roughly 4.3m/s (170in/s), which is safely less than the velocities that are likely in the flame.

The current signal that should be generated by such an experiment should form a pedestal with a width determined by the wire's duration in the flame, and with internal features determined by the length scale of the flame's micro-structures. If the wire processes with a speed of 4.3m/s (170in/s) through a 12mm (0.5in) flame, then the pedestal is approximately 2.8ms wide. The micro-structures that need to be resolved are probably determined by the number of individual flamelets formed at the tip's preheat openings. If we were to assume that these were so tightly spaced as 1mm, then the pedestal will contain features as fast as 0.2ms.

Time scales between 2.8ms and 0.2ms correspond to frequency content from 300Hz to 5kHz. Of course, these frequencies will scale with the disc speed. If these settings are respected, digital sampling must be *at least* 10kHz, and filtration below 5kHz must be avoided.

Were the diameter of the wire halved, so would the wire's thermal time constant, and the minimum disc speed would double. Because 400rpm was already an aggressive choice for a 0.25mm (.01in) wire, it should still be acceptable for a 0.12mm (.005in) diameter wire.

3 Total wire current

The theory of Clements and Smy establishes that the saturation current on a wire per area, J, is a function of the wire diameter, D_w, the fluid velocity, U, and the ion density, n. If J_D were defined to represent the saturation current per unit surface area a wire of diameter D would experience, then it is only a function of local ion density and bulk velocity. In this way, J_D is a locally defined fluid property from which the ion density may be deduced. Clearly, J_D is only a well defined property provided that all length scales of interest are larger than the diameter of the wire.

The value of J_D is readily measured directly by insertion of a wire into the fluid. When the fluid is uniform, the current measured, I, will be given by

$$I = \pi D_w L J_D$$

when L is the length of wire inserted into the plasma. This is the method used by MacLatchey [].

However, when the fluid is not uniform, a more sophisticated formulation is required. In general, J_D is a function in three dimensions; x and y perpendicular to the bulk velocity, and z parallel to the direction of flow. For the present work, we are entirely concerned with discerning the values of J_D in the $x-y$ plane (for a single value of z at a time). The method we establish here may be repeated at different values of z to produce complete three-dimensional maps for J_D.

Therefore, we may write, with sufficient generality for our needs, that

$$I = \pi D_w \int_0^R J_D(\vec{p}(r))\mathrm{d}r \tag{9}$$

when R is the radius of the spinning wire from the center of rotation, dr is the differential length along that radius, and $\vec{p}$ is a point along the path and an implicit function of r.

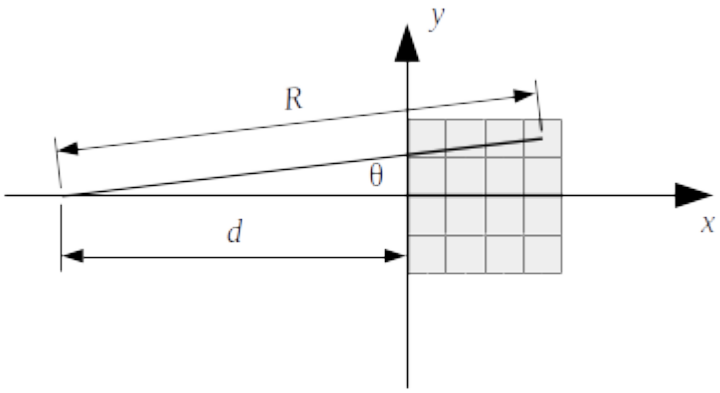

Figure 2: The measurement coordinate system with the measurement region shown in gray.

Inspection of Equation 9 is sufficient to conclude that a single measurement of I cannot distinguish between an infinite number of possible spatial distributions of J_D. Instead, it should be possible to deduce a specific J_D map by collecting a series of overlapping but dissimilar trajectories for the wire in x-y space.

As shown in Figure 2, a spinning disc with a wire probe could be passed through a flame with varying depths. When only the tip of the wire interacts with the flame, it would be certain that any electrical currents were collected at the wire's tip. Successively deeper passes through the flame could benefit from the prior measurements by subtracting the already known currents to infer the new currents realized at the wire's tip.

This approach would be akin to the Abel transformation used to infer an axis-symmetric quantity from a plurality of line-of-sight integrated measurements. However, there are a number of issues that plague a straight-forward application of the method as described. In order to evaluate the integral in Equation 9, it will become necessary to interpolate between the prior results of current measurements that will not lie precisely on the line formed by the wire. This calls for an interpolation scheme, but it is not immediately ob-

vious what artifacts may be introduced by such a method. It seems likely that small errors will accumulate from shallower measurements so that the deeper ones may suffer undesirable uncertainties.

Instead, we will adopt a more general problem: what field values of $J_D(x, y)$ minimize the error between many individual wire current measurements and wire currents calculated from the $J_D(x, y)$ field? While this preliminary statement makes no presumption on how the wire measurements were taken, as we see in Figure 2, wire current, $I(s, \theta)$, can be said to be a function of the center of rotation and the disc's angle. The fundamental problem is to calculate field values for J_D from many values of I. This approach takes advantage of how easily I can be calculated from J_D, makes no presumption that the signals are free of noise, and permits a disorganized cloud of individual measurements.

The error due to each measurement, $I_k(s_k, \theta_k)$, may be calculated

$$e_k = -I_k\left(s_k, \theta_k\right) + \pi D_w \int_0^R J_D\left(\vec{p}_k(r)\right) \mathrm{d}r \tag{10}$$
$$\vec{p}_k(r) = [x_k(r),\ y_k(r)]^T = [-s_k + r\cos(\theta_k),\ r\sin(\theta_k)]^T$$

When we use the method of least squares, we obtain a total error metric

$$E^2 = \sum_k {e_k}^2. \tag{11}$$

Now, we turn our attention to how the field of values for J_D should be constructed.

4 Grid

We will estimate values of J_D at nodes with uniform spacing, δ in both x and y directions. Though the choice of uniform spacing is not mandatory for this approach, it simplifies matters while sacrificing little generality. Our problem may be said to contain N_n nodes forming N_e $\delta \times \delta$ square elements when the array of nodes contains N_x x-values and N_y y-values, and

$$N_n = N_x N_y \tag{12}$$
$$N_e = (N_x - 1)(N_y - 1). \tag{13}$$

Nodes may be indexed either sequentially (using index n) from left-to-right and then bottom-to-top, or by x- and y-indices (using indices i and j). The

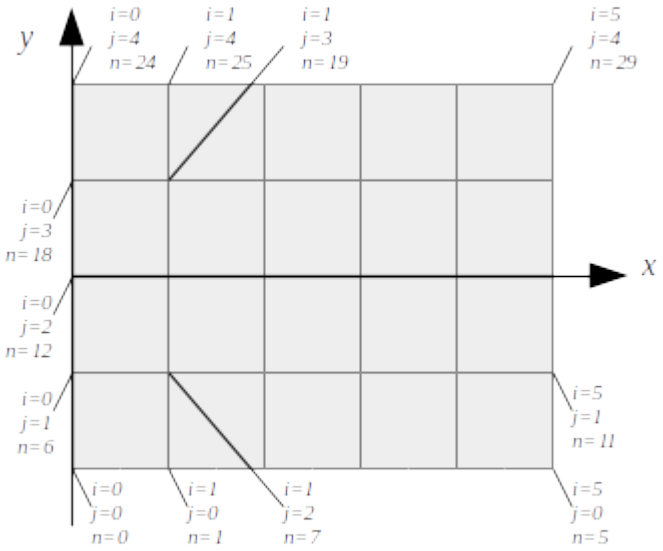

Figure 3: An example demonstrating the indexing schemes for nodes.

equivalent indices may be found

$$n = jN_x + i \tag{14}$$

$$j = \text{floor}(n/N_x) \tag{15}$$

$$i = n - jN_x \tag{16}$$

when $n \in [0, N_n - 1]$, $i \in [0, N_x - 1]$, and $j \in [0, N_y - 1]$.

This indexing scheme is depicted in Figure 3 with six columns and five rows of nodes.

We will take $\vec{X}$ to be a vector of all node values for J_D, which can be indexed either in sequential order, X_n, or by x- and y-indices, $X_{i,j}$. Elements are numbered to match the index of the node in the bottom-left corner, so that X_n is the bottom-left value of element (n). However, it is important to note that the top- and right-most elements cannot be evaluated since they will be missing nodes.

Once we have applied some interpolation scheme for approximating values of J_D, the integral of Equation 10 will be expressible as a vector dot product,

$$\int_0^R J_D(r, d, \theta)\mathrm{d}r = \vec{\Lambda}(R, d, \theta) \cdot \vec{X} \tag{17}$$

Though we have not yet established a means for calculating $\vec{\Lambda}$, when our choices for all $\vec{X}$ are optimal,

$$\begin{aligned}
0 &= \frac{\partial E^2}{\partial X_n} \\
&= \sum_k 2e_k \frac{\partial e_k}{X_n} \\
&= \sum_k \left(-I_k + \pi D_w \int_0^R J_D(r, d_k, \theta_k) \mathrm{d}r \right) \int_0^R \frac{\partial J_D(r, d_k, \theta_k)}{\partial X_n} \mathrm{d}r \\
&= -\sum_k I_k \vec{\Lambda}_k + \pi D_w \left[\sum_k \vec{\Lambda}_k \vec{\Lambda}_k \right] \cdot \vec{X}
\end{aligned} \tag{18}$$

This represents a matrix inversion problem for the calculation of the node values, $\vec{X}$. All that remains is to develop a means of calculating the interpolation vectors, $\vec{\Lambda}_k = \vec{\Lambda}(R, d_k, \theta_k)$, for a wire of radius, R, center of rotation, d_k, and angle, θ_k. In this way, there is a separate $\vec{\Lambda}$ vector for each raw measurement, k.

4.1 Interpolation

Each element is a finite domain in x, y space over which we may estimate the continuous function, J_D, at a point, $\vec{p} = [x, y]^T$, by linear interpolation of the node values.

$$\begin{aligned}
J_D(\vec{p}) = & \\
& X_{i,j}\, \phi_{00}(\vec{p}) + X_{i+1,j}\, \phi_{10}(\vec{p}) + \dots \\
& X_{i,j+1}\, \phi_{01}(\vec{p}) + X_{i+1,j+1}\, \phi_{11}(\vec{p})
\end{aligned} \tag{19}$$

when the ϕ functions are interpolation functions which we must define. Note that this is only valid when $\vec{p}$ lies within the element, so $x_i \le x \le x_{i+1}$ and $y_j \le y \le y_{j+1}$.

A formulation of the interpolation functions is facilitated by using a scaled coordinate system, $\hat{x} = (x - x_i)/(x_{i+1} - x_i)$, $\hat{y} = (y - y_j)/(y_{j+1} - y_j)$, or

$$[\hat{x}, \hat{y}]^T = \hat{\vec{p}} = \frac{\vec{p} - \vec{p}_{i,j}}{\delta}, \tag{20}$$

This constitutes a coordinate system with its origin at the bottom-left most node in the element (node n or equivalently node i, j) extending to $\hat{x} = 1$

at its right-most, and $\hat{y} = 1$ at its top most extent. These interpolation functions are *only* valid in that range.

For the interpolated values for J_D to agree with the node values at the verticies, each interpolation function must be one at its own node and zero at the other three. This implies four constraints on each interpolation function, permitting a four-term x, y polynomial. Using the element-scaled coordinate system, the resulting interpolation functions are

$$\phi_{00} = (1 - \hat{x})(1 - \hat{y}) \tag{21a}$$
$$\phi_{10} = \hat{x}(1 - \hat{y}) \tag{21b}$$
$$\phi_{01} = (1 - \hat{x})\hat{y} \tag{21c}$$
$$\phi_{11} = \hat{x}\hat{y} \tag{21d}$$

and may be more compactly written $\phi(\hat{\vec{p}})$. Note that each ϕ is unity when $\hat{\vec{p}}$ is at its respective node, but declines to zero at all other nodes.

4.2 Line Segments

Constructing the wire's path in space and the bounds on an element's regime in space is accomplished by defining line segments. In the case of elements, the four segments defining their boundary are simply defined by the segments connecting the nodes. In the case of the wire, the wire may be imagined to extend a radius, R, from the center of rotation at some angle relative to the x-axis.

It is convenient to define a line segment by a starting point, $\vec{p}_0$, and a direction, $\Delta\vec{p}$. Therefore, the line segment is defined as

$$\vec{p}(s) = \vec{p}_0 + s\Delta\vec{p} \qquad \forall\ s \in [0, 1]. \tag{22}$$

Negative values of s and values greater than 1 represented points projected beyond the bounds of the line segment. The value of s is related to the distance along the segment, r, by

$$r = s\|\Delta\vec{p}\|. \tag{23}$$

To calculate the location of an intersection between two line segments, a and b,

$$\vec{p}_a(s_a) = \vec{p}_{0,a} + s_a\Delta\vec{p}_a$$
$$\vec{p}_b(s_b) = \vec{p}_{0,b} + s_b\Delta\vec{p}_b,$$

we need only set the points $\vec{p}_a$ and $\vec{p}_b$ equal and solve for s_a and s_b. The problem is equivalent to

$$\vec{p}_{0,b} - \vec{p}_{0,a} = [\Delta\vec{p}_a,\ -\Delta\vec{p}_b] \cdot [s_a,\ s_b]^T \tag{24}$$

or, in terms of the individual x and y components,

$$\begin{bmatrix} x_{0,b} - x_{0,a} \\ y_{0,b} - y_{0,b} \end{bmatrix} = \begin{bmatrix} \Delta x_a & -\Delta x_b \\ \Delta y_a & -\Delta y_b \end{bmatrix} \begin{bmatrix} s_a \\ s_b \end{bmatrix} \tag{25}$$

There are five cases that can occur when searching for segment intersections:

1. If the determinant of the matrix, $\Delta x_b \Delta y_a - \Delta x_a \Delta y_b$ is zero, then the segments are parallel, and there is no solution,
2. If $0 \leq s_a \leq 1$ and $0 \leq s_b \leq 1$ then the segments intersect,
3. If $0 \leq s_a \leq 1$ but not s_b, then a projection of segment b intersects segment a,
4. If $0 \leq s_b \leq 1$ but not s_a, then a projection of segment a intersects segment b,
5. If neither s_a nor s_b is between 0 and 1, then only the projections of the segments intersect.

For line segments expressed within an element's dimensionless coordinate system,

$$\begin{aligned} \hat{\vec{p}}(s) &= \frac{\vec{p}(s) - \vec{p}_n}{\delta} = \hat{\vec{p}}_0 + s\Delta\hat{\vec{p}} \\ \hat{\vec{p}}_0 &= \frac{\vec{p}_0 - \vec{p}_n}{\delta} \\ \Delta\hat{\vec{p}} &= \frac{\Delta\vec{p}}{\delta}. \end{aligned} \tag{26}$$

This alternate formulation for a line segment is simply re-scaled by the elements size and offset by its bottom-left element's coordinates.

4.3 Calculating $\vec{\Lambda}$

Equation 18 reduces the deconvolution problem to a matrix inversion in terms of sums of $\vec{\Lambda}_k = \vec{\Lambda}(R, d_k, \theta_k)$ defined in Equation 17. Here, we use the interpolation functions to calculate $\vec{\Lambda}$ for the k data point with the disc center of rotation at $x = -d_k$, and the wire at an angle, θ_k. For each such wire location, elements may fall into three categories:

1. Elements through which the wire does not pass,

2. Elements with the wire passing through two faces,

3. An element with the wire passing through only one face.

The first will constitute the vast majority of elements for any given wire location and do not contribute to the integral. In this approach, we will consider each element that contains a segment of the wire, and we will accumulate their contributions to $\vec{\Lambda}$.

The integration of J_D over only the n element will contain contributions from the four nodes that form its limits,

$$\int_{(n)} J_D \mathrm{d}r = X_{i,j} \int_{(n)} \phi_{00} \mathrm{d}r + X_{i+1,j} \int_{(n)} \phi_{10} \mathrm{d}r + \ldots$$
$$X_{i,j+1} \int_{(n)} \phi_{01} \mathrm{d}r + X_{i+1,j+1} \int_{(n)} \phi_{11} \mathrm{d}r \tag{27}$$

Note that we have been quite deliberately vague with regard to the bounds on the integrals over r. Once we have isolated a line segment, $\vec{p}(s)$, within element n, each integral may be rescaled to be in terms of s,

$$\int_{(n)} \phi \mathrm{d}r = \|\Delta\vec{p}\| \int_0^1 \phi(\hat{p}(s)) \mathrm{d}s. \tag{28}$$

since $\mathrm{d}r = \|\Delta\vec{p}\| \mathrm{d}s$.

So, the four interpolation function integrals are

$$\begin{aligned}\Phi_{00} &= \int_0^1 \phi_{00}(s)\mathrm{d}s = \int_0^1 (1-\hat{x}_0 - s\Delta\hat{x})(1-\hat{y}_0 - s\Delta\hat{y})\mathrm{d}s \\ &= \frac{\Delta\hat{x}\Delta\hat{y}}{3} - \frac{\Delta\hat{x}(1-\hat{y}_0)}{2} - \frac{\Delta\hat{y}(1-\hat{x}_0)}{2} + (1-\hat{x}_0)(1-\hat{y}_0) \qquad (29a) \\ \Phi_{10} &= \int_0^1 \phi_{10}(s)\mathrm{d}s = \int_0^1 (\hat{x}_0 + s\Delta\hat{x})(1-\hat{y}_0 - s\Delta\hat{y})\mathrm{d}s \\ &= -\frac{\Delta\hat{x}\Delta\hat{y}}{3} + \frac{\Delta\hat{x}(1-\hat{y}_0)}{2} - \frac{\Delta\hat{y}\hat{x}_0}{2} + \hat{x}_0(1-\hat{y}_0) \qquad (29b) \\ \Phi_{01} &= \int_0^1 \phi_{01}(s)\mathrm{d}s = \int_0^1 (1-\hat{x}_0 - s\Delta\hat{x})(\hat{y}_0 + s\Delta\hat{y})\mathrm{d}s \\ &= -\frac{\Delta\hat{x}\Delta\hat{y}}{3} - \frac{\Delta\hat{x}\hat{y}_0}{2} + \frac{\Delta\hat{y}(1-\hat{x}_0)}{2} + (1-\hat{x}_0)\hat{y}_0 \qquad (29c) \\ \Phi_{11} &= \int_0^1 \phi_{11}(s)\mathrm{d}s = \int_0^1 (\hat{x}_0 + s\Delta\hat{x})(\hat{y}_0 + s\Delta\hat{y})\mathrm{d}s \\ &= \frac{\Delta\hat{x}\Delta\hat{y}}{3} + \frac{\Delta\hat{x}\hat{y}_0}{2} + \frac{\Delta\hat{y}x_0}{2} + \hat{x}_0\hat{y}_0 \qquad (29d)\end{aligned}$$

Finally, we may construct $\vec{\Lambda}$ in terms of these Φ formulae. Here, the contribution to each $\vec{\Lambda}$ element from only element n is

$$\Lambda_{i,j}^{(n)} = \|\Delta\vec{p}\|\Phi_{00} \qquad (30a)$$

$$\Lambda_{i+1,j}^{(n)} = \|\Delta\vec{p}\|\Phi_{10} \qquad (30b)$$

$$\Lambda_{i,j+1}^{(n)} = \|\Delta\vec{p}\|\Phi_{01} \qquad (30c)$$

$$\Lambda_{i+1,j+1}^{(n)} = \|\Delta\vec{p}\|\Phi_{11} \qquad (30d)$$

and zero otherwise. The total $\vec{\Lambda}$ vector is constructed by summing these values contributed from all the elements.

$$\Lambda_{i,j} = \sum_n \Lambda_{i,j}^{(n)} \qquad (31)$$